

# A search for sub-second radio variability predicted to arise toward 3C 84 from intergalactic dispersion

C. A. Hales

*National Radio Astronomy Observatory, P.O. Box 0, Socorro, NM 87801, USA*

W. Max-Moerbeck

*National Radio Astronomy Observatory, P.O. Box 0, Socorro, NM 87801, USA*

*Max-Planck-Institut für Radioastronomie, Auf dem Hügel 69, D-53121 Bonn, Germany*

D. A. Roshi

*National Radio Astronomy Observatory, Charlottesville & Green Bank, 520 Edgemont Road, Charlottesville, VA 22903, USA*

and

M. P. Rupen

*National Research Council of Canada, Herzberg Astronomy and Astrophysics, Dominion Radio Astrophysical Observatory, P.O. Box 248, Penticton, BC V2A 6J9, Canada*

## ABSTRACT

We empirically evaluate the scheme proposed by Lieu & Duan (2013) in which the light curve of a time-steady radio source is predicted to exhibit increased variability on a characteristic timescale set by the sightline’s electron column density. Application to extragalactic sources is of significant appeal as it would enable a unique and reliable probe of cosmic baryons. We examine temporal power spectra for 3C 84 observed at 1.7 GHz with the Karl G. Jansky Very Large Array and the Robert C. Byrd Green Bank Telescope. These data constrain the ratio between standard deviation and mean intensity for 3C 84 to less than 0.05% at temporal frequencies ranging between 0.1–200 Hz. This limit is 3 orders of magnitude below the variability predicted by Lieu & Duan (2013) and is in accord with theoretical arguments presented by Hirata & McQuinn (2014) rebutting electron density dependence. We identify other spectral features in the data consistent with the slow solar wind, a coronal mass ejection, and the ionosphere.

*Subject headings:* intergalactic medium — large-scale structure of universe — radiation mechanisms: general — radio continuum: general — solar wind — Sun: coronal mass ejections (CMEs)

## 1. Introduction

Approximately 30% of all baryons in the low redshift ( $z \lesssim 1$ ) Universe remain unaccounted for observationally. Simulations predict that the bulk, if not all, of these ‘missing baryons’ reside at shock-heated temperatures between  $10^5$  K to  $10^7$  K in the diffuse warm-hot intergalactic medium (WHIM) of the mildly non-linear cosmic web (Cen & Ostriker 1999; Davé et al. 2001; Bregman 2007; Shull et al. 2012). Similar temperatures may also be present in voids (Chang et al. 2012, 2014; Menzler & Schlickeiser 2015). Detecting gas under these conditions is challenging. Emission and absorption based probes such as the Sunyaev-Zel’dovich effect and spectral line diagnostics, in combination with gravitational lensing and cross-correlation studies, are becoming increasingly sensitive to the WHIM (e.g. Buote et al. 2009; Brown et al. 2010; Dietrich et al. 2012; Gralla et al. 2014; Génova-Santos et al. 2015; Tejos et al. 2016). However, these tracers are complicated by degeneracies with physical conditions including temperature, density structure, metallicity, magnetic field, and ionization state.

An alternate tracer that provides equal sensitivity to every free electron along the line of sight, irrespective of gas condition, is the dispersion measure,  $DM = \int n_e(z) dl$ , where  $n_e(z)$  is the electron density as a function of redshift and  $dl$  is differential proper distance. Radio band observations of the frequency-dependent arrival times from an impulsive event, such as a pulsar pulse, can be used to infer the DM. Given that the Universe is essentially fully ionized at  $z < 2.5$  (McQuinn et al. 2009), intergalactic DMs offer excellent prospects for mapping baryons throughout large scale structure including the WHIM. The challenge to date, however, has been the lack of suitable extragalactic targets. Pulsar DMs have been used to successfully map ionized gas throughout the Milky Way (Cordes & Lazio 2002), but pulsars are too faint to be detected beyond  $\sim 100$  kpc. Variable radio emission from quasars and gamma-ray bursts has been proposed (e.g. Haddock & Sciama 1965; Palmer 1993), but the lightcurves for these sources do not contain suitably sharp features against which to measure dispersive delays.

Excitingly, this situation may have improved with the discovery of a new population. Fast radio bursts (FRBs) are bright, isolated, highly dispersed, millisecond-duration flashes of unknown astrophysical origin, discovered with single-dish radio telescopes and inferred to have a high all-sky event rate (Lorimer et al. 2007; Thornton et al. 2013; Keane & Petroff 2015). Their large dispersion measures are consistent with a population of standard candles observable to  $z \lesssim 1$  (Luan & Goldreich 2014; Dolag et al. 2015), though less distant candidates located within  $z \lesssim 0.1$  (Cordes & Wasserman 2016; Pen & Connor 2015) or even purely within our Galaxy (Maoz et al. 2015) may also explain their observed properties. Keane et al. (2016) recently claimed the first localization of an FRB, using the detection

of a fading radio transient to identify the host as an elliptical galaxy at  $z = 0.492$ . However, their FRB–afterglow association has been strongly disputed as likely arising from scintillation of an unrelated background active galactic nucleus (Williams & Berger 2016; Akiyama & Johnson 2016). Spitler et al. (2016) subsequently report in a separate work the discovery of a repeating FRB, supporting an origin in a nearby extragalactic ( $z \lesssim 0.1$ ) neutron star. Spitler et al. (2016) note that the non-detection of repeating bursts from other FRBs may indicate the existence of more than one mechanism for producing FRBs. If an additional class of FRB hosts can be ranged to cosmological distances (e.g. Fender & Oosterloo 2015; Margalit & Loeb 2015), their DMs can be used to address a range of science. Examples include mapping the three-dimensional distribution and clustering of cosmic baryons (Masui & Sigurdson 2015), quantifying the accretion onto and feedback within galactic halos (McQuinn 2014), measuring the intergalactic baryon mass fraction (Deng & Zhang 2014), constraining the dark energy equation of state (Gao et al. 2014; Zhou et al. 2014), providing insights into turbulence in the intergalactic medium and the origin and evolution of cosmic magnetism by helping to unravel the degeneracy between electron density and magnetic field strength in Faraday rotation measures (Donnert et al. 2009; Ryu et al. 2012; Akahori et al. 2016), and possibly probing He II reionization at  $z \sim 3$  if a population of FRBs is present up to these redshifts (Zheng et al. 2014).

Access to the science above could also be gained through the development of new observational techniques. Pursuing this strategy, Lieu & Duan (2013) and Lovelace & Richards (2013) raised the revolutionary prospect of measuring DMs toward time-steady rather than impulsive sources. These works predict the appearance of fluctuations in the light from distant radio sources on timescales of milliseconds, with the characteristic timescale for each source proportional to its DM. If correct, these schemes would enable the cosmic baryon science above to be addressed using known populations, such as radio quasars with confirmed ranges out to and beyond  $z \sim 4$ . However, a comprehensive theoretical rebuttal was subsequently presented by Hirata & McQuinn (2014), ruling out any expected dependence between DM and the statistical properties of radiation received from a time-steady radio source. Hirata & McQuinn (2014) derive the 2- and 4-point correlation of the received electric field (including examination of the quantum nature of the electromagnetic field for the latter), corresponding to the Lovelace & Richards (2013) and Lieu & Duan (2013) techniques respectively. They demonstrate under general principles that the former is insensitive to DM, and the latter has extremely weak dependence due to the central limit theorem for a large number of incoherently emitting electrons.

In this work we present an independent empirical evaluation of the technique proposed by Lieu & Duan (2013); we do not evaluate the technique proposed by Lovelace & Richards (2013) due to challenging sensitivity criteria. While the theoretical results of Hirata & McQuinn

(2014) convincingly rule out the need for empirical examination, we present the findings of our customized observations here as an independent approach and as a demonstration of the ancillary science available through fast cadence radio observations. Section 2 describes our experiment design. Section 3 describes our radio observations and data reduction. Results are presented in Section 4 with discussion in Section 5. We conclude in Section 6.

## 2. Experiment Design

The techniques proposed by Lieu & Duan (2013) and Lovelace & Richards (2013) are based on the plasma dispersion effect whereby photon wave packets undergo broadening in their envelope width and a drift in their carrier frequency as they traverse vast spans of the ionized intergalactic medium. Both works argue that the statistical properties of radiation received from a time-steady incoherent source will be altered in the presence of plasma dispersion, provided the radiation is composed of many temporally overlapping wave packets (e.g. synchrotron). Lieu & Duan (2013) predict that, in the case of no intervening plasma, strong intensity fluctuations will be observed with standard deviation half<sup>1</sup> the mean intensity of the source,  $\sigma_I = \bar{I}/2$ , and correlation timescale given by the inverse of the observation bandwidth,  $\tau_c = (2\pi\Delta\nu)^{-1}$ . When dispersive plasma is present, they predict intensity fluctuations spread over a range of timescales. Fourier power is predicted to rise monotonically from  $\tau_c$  until exhibiting the full plasma-free variability level ( $\sigma_I = \bar{I}/2$ ) at a ‘stretched envelope’ timescale given by

$$\tau_{\text{env}} = \sqrt{2} \tau_c \left\{ 1 + \left[ 5 \times 10^6 \left( \frac{\Delta\nu/\nu_0}{10^{-2}} \right)^2 \left( \frac{\nu_0}{1 \text{ GHz}} \right)^{-1} \left( \frac{\text{DM}}{10^3 \text{ pc cm}^{-3}} \right) \right]^2 \right\}^{1/2} \text{ [s]} \quad (1)$$

for central observing frequency  $\nu_0$ . Similarly, Lovelace & Richards (2013) predict that plasma dispersion will cause a peak to appear in the two-point correlation of the electric field between two nearby frequencies.

To empirically test the behavior predicted by Lieu & Duan (2013), we seek to analyze radio-band light curves of a target with known DM. To minimize any possible confusion with rapid variability caused by ionospheric, interplanetary, or interstellar scintillation (e.g. Smith 1950; Clarke 1964; Hewish et al. 1964; Dennett-Thorpe & de Bruyn 2002), we require sampling on sub-second timescales (intergalactic scintillation timescales are many orders of magnitude larger and thus negligible here; Pallottini et al. 2013). This in turn requires a strong radio source to ensure high signal to noise within short integration periods.

---

<sup>1</sup>In a follow-up paper, Lieu et al. (2013) give the standard deviation as the mean intensity of the source.

For this purpose we select 3C 84, the radio source associated with the giant elliptical galaxy NGC 1275, located at  $z = 0.018$  at the center of the brightest X-ray cluster in the sky, Perseus. 3C 84 is one of the strongest and most compact radio sources in the sky (Pauliny-Toth et al. 1976). While 3C 84 is known to be variable on timescales of years (Dent 1966; Abdo et al. 2009), we do not expect any intrinsic sub-second variability because the light crossing time for its  $3.4 \times 10^8 M_\odot$  black hole (Wilman et al. 2005) is  $\sim 1$  hour (though cf. plausible rapid variability due to opacity variations described by Marscher 1979 and subhorizon-scale black hole lightning described by Aleksić et al. 2014).

We calculate the total DM along the line of sight to 3C 84 as follows. The contribution from the intracluster medium within Perseus is estimated to be  $2700 \text{ pc cm}^{-3}$ . This is obtained by integrating the electron density profile inferred from X-ray observations. We model this profile with a mean value  $0.3 \text{ cm}^{-3}$  within radius  $r < 2 \text{ kpc}$  (Taylor et al. 2006) that declines beyond as  $0.31(r/\text{kpc})^{-0.86}$  out to  $r = 200 \text{ kpc}$  (Fabian et al. 1981, 2006). The foreground Milky Way contribution is approximately  $100 \text{ pc cm}^{-3}$  (Cordes & Lazio 2002). The total DM is therefore approximately  $2800 \text{ pc cm}^{-3}$ . We place overly conservative lower and upper limits on this total DM of  $1500 \text{ pc cm}^{-3}$  and  $6000 \text{ pc cm}^{-3}$ , respectively. These limits are intended to account for all plausible uncertainties, including additional DM contributions due to the intergalactic path between Perseus and our Galaxy (likely  $< 100 \text{ pc cm}^{-3}$ ; Ioka 2003; McQuinn 2014), contributions local to NGC 1275, and differences between our line of sight and the in-sky X-ray profile used to estimate the dominant intracluster medium contribution (the halo geometry is likely non-spherical; Pedlar et al. 1990).

To mitigate potential instrumental systematics, we pursue observations with two independent facilities: the Karl G. Jansky Very Large Array (VLA) and the Robert C. Byrd Green Bank Telescope (GBT). The maximum throughput of the VLA’s WIDAR correlator is approximately  $1 \text{ TB hr}^{-1}$ . Access to this data rate is only available through non-standard correlator configurations. The special mode commissioned by Law et al. (2015) for FRB studies provides  $5 \text{ ms}$  time resolution for  $2 \times 128 \text{ MHz}$  spectral windows at L-band. We make use of this mode here as it is well matched to our experiment. We pursue observations with the GBT’s VEGAS backend in Mode 1 with  $2.5 \text{ ms}$  sampling.

We tune our observing setup as follows. We set the requirement  $\tau_{\text{env}} < 40 \text{ Hz}$  so that Fourier behavior on faster timescales (toward  $\tau_c$ ) can be gleaned up to the  $100 \text{ Hz}$  Nyquist frequency accessible with the VLA (up to  $200 \text{ Hz}$  is accessible with  $2.5 \text{ ms}$  sampling at the GBT). We seek observing frequencies near  $1760 \text{ MHz}$  to avoid typical radio frequency interference (RFI) at the VLA and GBT sites. To satisfy these requirements with the DM range predicted above, according to Equation (1) we require  $\Delta\nu = 8 \text{ MHz}$  ( $\tau_c = 20 \text{ ns}$ ). For this setup, Equation (1) therefore predicts  $\tau_{\text{env}}$  in the range  $10 - 40 \text{ Hz}$ , with  $22 \text{ Hz}$

corresponding to  $DM = 2800 \text{ pc cm}^{-3}$ . The largest bandwidth for which  $\tau_{\text{env}}$  will remain on sub-second timescales is  $\Delta\nu = 90 \text{ MHz}$  ( $\tau_c = 2 \text{ ns}$ ). For this bandwidth, Equation (1) predicts  $\tau_{\text{env}} = 1 - 4 \text{ Hz}$ , with 2 Hz corresponding to  $DM = 2800 \text{ pc cm}^{-3}$ .

We do not investigate the predictions from Lovelace & Richards (2013) in this work. This is due to challenges in meeting signal to noise requirements within narrow channel bandwidths at high time resolution, which can only be overcome by combining channels in a customized filter bank (similar to those used in pulsar astronomy). While possible, we did not ultimately pursue this strategy due to the findings from Hirata & McQuinn (2014) and the conclusions reported in this work for the Lieu & Duan (2013) experiment.

### 3. Observations and Data Reduction

Observations of 3C 84 are summarized in Table 1. The on-target duration was approximately 5 min per epoch. We observed the flux density calibrator 3C 48 in each session.

We initially performed simultaneous observations with the VLA and GBT on 2014 April 11. Unfortunately, these VLA data were corrupted due to a correlator error. Successful observations with the VLA were subsequently obtained on 2014 May 15. Additional VLA observations were obtained on 2015 January 2 at large solar elongation to discriminate the effects of interplanetary scintillation in the low-elongation 2014 VLA and GBT data.

Specifics of the observations and data reduction procedures for each facility are detailed as follows.

Table 1: Observations of 3C 84.

Facility	Configuration	Project Code	Epoch (UTC)	Solar Elongation ( $^{\circ}$ )
GBT	–	14A-418	2014 Apr 11 14:18	43
VLA	A	14A-409	2014 May 15 15:28	23
VLA	C	14B-503	2015 Jan 02 00:10	133

### 3.1. Very Large Array

VLA observations were performed using the correlator mode developed by Law et al. (2015), delivering dual circular polarization products in two spectral windows at 5 ms time resolution. We centered these spectral windows at 1410 and 1760 MHz, each spanning  $64 \times 2$  MHz channels. Results from the 1410 MHz window are consistent with the 1760 MHz window and will not be described further in this work (the dual-window setup was originally intended to evaluate the proposed frequency dependence for  $\tau_{\text{env}}$ ).

The data were reduced using standard tasks in version 4.3.0 of the CASA package (McMullin et al. 2007). Hanning smoothing was applied. Only a few percent of the data were found to be affected by RFI. These were manually identified and flagged. Our final results are unaffected if the Hanning smoothing step is removed, due to the minimal presence of RFI in the data. Flux density calibration was bootstrapped against 3C 48, adopting the most recent 2012 value from the Perley & Butler (2013) standard. Phase calibration was performed for each 5 ms integration for both 3C 48 and 3C 84 to verify data fidelity and to remove positional shifts due to scintillation in preparation for image-based analysis. The solar elongations for 3C 48 at the 2014 and 2015 epochs were  $28^\circ$  and  $112^\circ$ , respectively.

We extracted 120 s of continuous 3C 84 sampling within two bandwidths, spanning 8 MHz and 90 MHz, from both the 2014 and 2015 data. Central frequencies for the 8 MHz bands were selected to ensure they did not exhibit any RFI over the duration of the observations. The 90 MHz bands were selected to minimize the inclusion of any spectral channels where RFI had been flagged. These selections resulted in slightly different central frequencies for the two bandwidths. The central frequencies for the 8 MHz bandwidth data are 1765 MHz and 1761 MHz for the respective consecutive epochs. The corresponding central frequencies for the 90 MHz bandwidth data are 1759 MHz and 1757 MHz. Differences in predicted  $\tau_{\text{env}}$  are negligible. Light curves were constructed by imaging each 5 ms integration and measuring 3C 84’s flux density using the peak surface brightness. The observed noise per integration is approximately  $77 \text{ mJy beam}^{-1}$  for the 8 MHz data and  $23 \text{ mJy beam}^{-1}$  for the 90 MHz data, consistent with theoretical predictions.

Extensive diagnostic checks were performed throughout this process to search for and identify any spurious instrumentally-induced signatures, for example a tone identified at 4 Hz that was traced to a memory failure in the delay module on the station board for antenna EA09.



### 3.2. Green Bank Telescope

GBT observations were performed with the VEGAS<sup>2</sup> backend using Mode 1, delivering dual linear polarization data spanning the frequency range 0.8–2.3 GHz split into 1024 spectral channels. The maximum useable bandwidth at L-band is limited by the feed to 650 MHz. Of this, we restricted our calibration to the range 1704–1814 MHz and focused our experimental analysis on two bands spanning 6 ( $\approx 8$  MHz) and 62 ( $\approx 90$  MHz) channels centered at approximately 1736 MHz and 1759 MHz, respectively. We selected the central frequency of the 8 MHz band to be as close as possible to 1760 MHz while avoiding any RFI. Differences in predicted  $\tau_{\text{env}}$  due to the different frequency and bandwidth selections, and compared to the VLA observations, are negligible.

We performed two types of observations. First, we observed 3C 48 and 3C 84 at 1 s time resolution with noise diode switching enabled (1 s period with power  $\sim 10\%$  of the system temperature). We then repeated these observations using 2.5 ms time resolution, but with noise diode switching turned off to prevent data blanking. In both cases we employed position switching with reference points located 45' north of 3C 48 and 45' south of 3C 84. These positions are devoid of sources in the 1.4 GHz NRAO VLA Sky Survey (Condon et al. 1998) and exhibit negligible-gradient background 408 MHz brightnesses within approximately 2% of the target position values (Haslam et al. 1982).

The data were calibrated independently per polarization. The absence of the noise diode signal required a non-standard calibration which we implemented in Python based on the GBTIDL<sup>3</sup> procedures outlined by Braatz (2009). Only a few percent of the data in our frequency range of interest were found to be affected by RFI. These data were manually identified and flagged. We used Equation (1) from Braatz (2009) to calculate the time-averaged system temperature,  $T_{\text{sys}}$ , for each of 3C 48 and 3C 84 using the 1 s data. We used Equation (2) from Braatz (2009) to calculate the time-averaged antenna temperature as a function of spectral channel,  $T_{\text{ant}}(\nu)$ , for 3C 48 using the 1 s data. To calculate the antenna temperature as a function of time and channel for 3C 84 using the 2.5 ms data,  $T_{\text{ant},\text{sig}}(t, \nu)$ , we first calculated the following modified system temperature to account for the absence of the noise diode signal,

$$T'_{\text{sys}} = T_{\text{sys}} \left\langle \frac{(\overline{\text{sig}} - \overline{\text{ref}})}{\overline{\text{ref}}} \middle/ \frac{(\overline{\text{sig}_{\text{caloff}}} - \overline{\text{ref}_{\text{caloff}}})}{\overline{\text{ref}_{\text{caloff}}}} \right\rangle, \quad (2)$$

where  $\text{sig} \equiv \text{sig}(t, \nu)$  and  $\text{ref} \equiv \text{ref}(t, \nu)$  are position-switched target and reference data,

---

<sup>2</sup><http://www.gb.nrao.edu/vegas/modes>

<sup>3</sup><http://gbtidl.nrao.edu>



respectively, bars and angular brackets indicate time and channel averages, respectively, and the caloff subscripts indicate 1 s data where the calibration noise diode is off. We then calculated

$$T_{\text{ant,sig}}(t, \nu) = T'_{\text{sys}} \frac{\text{sig} - \overline{\text{ref}}}{\overline{\text{ref}}}, \quad (3)$$

and similarly  $T_{\text{ant,ref}}(t, \nu)$  for the reference position with sig replaced by ref. We confirmed this strategy by calculating Equation (3) for 3C 48 using the 2.5 ms data. The result was consistent with the original  $T_{\text{ant}}$  derived from the 1 s data.

The data for both linear polarizations were then averaged. Corrected antenna temperatures were calibrated to the most recent 2012 flux density for 3C 48 from the Perley & Butler (2013) standard. Channels were averaged to form our two bands of interest. From these, we extracted 85 s of continuous sampling for 3C 84. We calculate the noise in our data by integrating the power spectrum for each light curve between 100 Hz and the 200 Hz Nyquist frequency, excluding lower temporal frequencies that are dominated by real signal (see Fig. 2 presented shortly). The observed noise per sample is approximately 220 mJy beam<sup>−1</sup> for the 8 MHz data and 66 mJy beam<sup>−1</sup> for the 90 MHz data, consistent with theoretical predictions.

We examined the 1 s reference position data for evidence of gain fluctuations in the receiver that would appear as flicker noise (Mason 2013). If present, such fluctuations could potentially be misidentified as having a non-instrumental origin. We found no evidence for flicker noise above a temporal frequency of 0.07 Hz. We found tentative evidence for increased spectral power below 0.07 Hz. This temporal frequency is much lower than the timescales of interest in this work. Additionally, our primary interest in this work regards the 2.5 ms data for which the thermal noise is greater. To avoid any possible confusion, in this work we only focus on temporal frequencies greater than 0.1 Hz.

## 4. Results

The VLA and GBT light curves of 3C 84 are displayed in Fig. 1. The mean flux densities of the 8 MHz and 90 MHz bandwidth data differ at each given epoch due to their slightly different central frequencies and the spectrum of 3C 84. Our data indicate that this spectrum is falling<sup>4</sup> as a function of frequency (e.g. Nagai et al. 2009). Comparing between epochs, the mean flux densities of the GBT data are higher than the VLA data, and there is a slight increase between the 2014 and 2015 VLA data. The former difference is due to extended structure about 3C 84 to which our interferometric observations are insensitive;

---

<sup>4</sup>Historically this has not always been the case at our observing frequency (e.g. Berlin et al. 1980).

3C 84 is located within a  $5'$  halo at 1.4 GHz (Maltby & Moffet 1962; Ryle & Windram 1968). The difference between the 2014 and 2015 epochs is caused by two factors. First, the 2015 data were obtained in C configuration, delivering increased sensitivity to the extended halo compared to the 2014 A configuration data. Second, 15 GHz pointing calibration data from the Very Long Baseline Array (VLBA) indicate that 3C 84 underwent a flare that peaked approximately 2014 July, with flux density at our 2015 epoch a few percent higher compared to the 2014 epoch. A third (opposite) contribution could arise from our adoption of a fixed 2012 flux density for 3C 48. If the flux density of 3C 48 has continued to decline following the historical trend shown by Perley & Butler (2013), our flux densities for 3C 84 will be underestimated, though by no more than about 2% at the 2015 epoch. The conclusions presented in this work are not affected by the differences in mean flux densities seen in Fig. 1.

Fig. 2 displays power spectra<sup>5</sup> for the light curves sampled in Fig. 1. From high to low temporal frequencies, the spectra are characterized by flat power levels that rise to a plateau. The observed power at high frequencies is limited by sensitivity, as evidenced by expected lower power levels for the 90 MHz bandwidth data compared to the 8 MHz data and similarly between the VLA and GBT data. At lower frequencies as the spectra rise, correspondence between the 8 MHz and 90 MHz data improves, indicating Fourier power dominated by signal and not noise. The difference between the GBT target and reference data at low frequencies indicates that the increased Fourier power is real (for clarity, only the 8 MHz reference data is shown in Fig.’s 1 and 2; the 90 MHz reference data exhibit the same trends). The difference in power levels between the GBT target and reference 8 MHz data at high frequencies is consistent with increased noise due to the presence of the  $5'$  halo about 3C 84; the system temperature calculated at the reference position (used for calibration) is a factor 3 smaller than a similarly calculated system temperature at the position of 3C 84.

The curves displayed in Fig. 2 are informal fits to guide the eye. The dotted and dashed curves characterize the GBT and 2014 VLA data, respectively, using a power law with common slope -4.8. The dotted curve flattens at 2.3 Hz while the dashed curve flattens at 1.5 Hz. These frequencies correspond to the strongest fluctuations seen on  $\sim 0.5$  s timescales in Fig. 1. The dot-dashed curve characterizes both the GBT reference position data and 2015 VLA data using a power law with slope -1.4 that flattens at 0.25 Hz.

We place a conservative upper limit on the presence of any signals in the 10–40 Hz range by injecting sine waves with specified amplitude into the 8 MHz light curves, as described

---

<sup>5</sup>We calculate power spectra as the modulus squared of the discrete Fourier transform, normalized such that the sum over positive frequencies is equal to the variance of the input light curve.

in the caption to Fig. 2. At all epochs we limit the standard deviation of fluctuations to less than 0.05% of the mean intensity. Examining the GBT and 2015 VLA data, the standard deviation to mean ratio is less than 0.05% over the full 0.1–200 Hz range. Similar calculations in the 1–4 Hz range (or indeed over the full 0.1–200 Hz range) for the 90 MHz light curves yield a consistent result. For reference, the variability predicted by the theory of Lieu & Duan (2013) would appear in Fig. 2 at power levels near 100 Jy<sup>2</sup>.

## 5. Discussion

### 5.1. Implications for Proposed Theory

Our empirical limits on variability in the 1–4 Hz and 10–40 Hz ranges for 3C 84 are 3 orders of magnitude less than the levels predicted by the theory of Lieu & Duan (2013). We do not see any evidence for a decline in spectral power between these frequencies and our highest observed frequency at 200 Hz. These results support the theoretical conclusion by Hirata & McQuinn (2014) that the scheme proposed by Lieu & Duan (2013) is insensitive to dispersion measure.

### 5.2. Origins of Increased Spectral Power Below 10 Hz

We associate the increased spectral power indicated by the dotted and dashed curves in Fig. 2 with scintillation caused by the interplanetary medium. We associate the dot-dashed curves with ionospheric scintillation. We justify these associations as follows.

The dotted and dashed curves in Fig. 2 are consistent with power spectra for interplanetary scintillation reported throughout the literature, for example Mejia-Ambriz et al. (2015) who observed 3C 48 at 140 MHz and 327 MHz during the current peak of Solar Cycle 24 at similar elongations to our data. The frequency at the knee where the curves change slope corresponds to the Fresnel filter frequency,  $f_F$ , which is in turn proportional to the velocity of the solar wind (e.g. Manoharan & Ananthakrishnan 1990). The solar-wind velocity projected onto the plane perpendicular to the line of sight can be estimated as  $V_{\perp} \approx f_F \sqrt{\pi \lambda A \cos(\epsilon)}$  where  $\lambda$  is the observing wavelength,  $A$  is 1 AU, and  $\epsilon$  is solar elongation. Taking  $f_F = 1.5$  Hz from § 4 and  $\epsilon = 23^\circ$  from Table 1 we estimate  $V_{\perp} \approx 410$  km s<sup>−1</sup> at the 2014 May 15 epoch. This is consistent with the  $\sim 400$  km s<sup>−1</sup> velocity of the slow solar wind (e.g. Feldman et al. 2005). The data at the 2014 Apr 11 epoch (dotted curve) exhibit excess power compared to 2014 May 15 (dashed curve), appearing shifted to the right with  $f_F \approx 2.3$  Hz and thus  $V_{\perp} \approx 570$  km s<sup>−1</sup>. The cause of this shift is likely the large coronal

mass ejection CME52 that departed the Sun at 2014 Apr 8 23:12 UTC in the direction of 3C 84 with median velocity  $488 \text{ km s}^{-1}$  and velocity range  $230\text{--}900 \text{ km s}^{-1}$ , as reported in the CACTus<sup>6</sup> quicklook catalog for the LASCO instrument onboard the *Solar and Heliospheric Observatory* (Robbrecht & Berghmans 2004). For reference, ejecta traveling at  $600 \text{ km s}^{-1}$  oriented perpendicular to the line of sight to the sun would have traversed 3C 84’s position at the time of our GBT observations.

Interplanetary scintillation is unlikely to be the origin of the excess power observed at the GBT reference position on 2014 Apr 11, indicated by the dot-dashed curve in Fig. 2. This is because we expect Galactic emission at the reference position to be mostly smooth on the angular scales  $\lesssim 1''$  required for interplanetary scintillation (Hewish et al. 1964). Instead, we attribute the excess power to ionospheric scintillation where the critical angular scale is  $\lesssim 2'$  (given by the Fresnel scale  $\sqrt{\lambda d}$  at the height of the ionosphere  $d \approx 400 \text{ km}$ ). The dot-dashed curve is consistent with power spectra for ionospheric scintillation reported in the literature, for example Fang et al. (2012) who present spectra with  $f_F \approx 0.14 \text{ Hz}$  and power law slope  $\approx -1.8$  from observations of *Global Positioning System* satellites. Their data were obtained in 2008–2009 during solar minimum. Our higher Fresnel frequency at  $0.25 \text{ Hz}$  is likely due to increased solar activity in 2014–2015. We also attribute the excess power observed on 2015 Jan 2 to ionospheric scintillation. Interplanetary scintillation is insufficient to explain this power due to the large solar elongation of 3C 84 and the expected  $\epsilon^{-4}$  dependence for interplanetary scattering power (Armstrong & Coles 1978). Finally, we tentatively note that the Fresnel frequency associated with the GBT reference position data may be slightly higher than for the 2015 VLA data. This could possibly be due to the class C9.4 solar flare emitted 3 hours prior to our GBT observation, as cataloged by the X-ray Sensor on board the *GOES-15* satellite<sup>7</sup> (Garcia 1994). For comparison, no flares greater than class C2.1 were observed in the 24 h preceding our 2015 observation.

## 6. Conclusions

We examined high cadence VLA and GBT observations of 3C 84 at  $1.7 \text{ GHz}$  for signatures of intergalactic dispersion predicted by Lieu & Duan (2013). Our data constrain the ratio between standard deviation and mean intensity for 3C 84 to a conservative upper limit of  $0.05\%$  over timescales spanning  $0.1\text{--}200 \text{ Hz}$ . This limit is 3 orders of magnitude less than predicted, specifically within the  $1\text{--}4 \text{ Hz}$  and  $10\text{--}40 \text{ Hz}$  ranges appropriate for 3C 84’s DM

---

<sup>6</sup><http://sidc.oma.be/cactus/>

<sup>7</sup><http://www.ngdc.noaa.gov/stp/satellite/goes/>

and our two observational setups.

Our finding is consistent with the theoretical analysis of Hirata & McQuinn (2014), who concluded that the scheme proposed by Lieu & Duan (2013) (and similarly by Lovelace & Richards 2013) is insensitive to dispersion measure. We note that, had the theory been correct, it is plausible that indicative signatures could have escaped detection throughout historical radio observations due to the subtle predicted dependencies on bandwidth and source DM (e.g. the dedicated high cadence search for anomalous variability from 3C 84 by Harp et al. 2015).

We investigated the origins of increased temporal spectral power below 10 Hz in our data. We found contributions consistent with the slow solar wind, a coronal mass ejection, the ionosphere, and possibly the excited ionosphere perturbed by a solar flare.

Our variability limit for 3C 84 demonstrates that signal paths through the VLA’s WIDAR correlator and the GBT’s VEGAS backend are of high fidelity. We limit the presence of any contaminating artifacts to the equivalent of a sinusoid with amplitude  $< 10$  mJy and frequency in the range 0.1–200 Hz for observations at  $> 2.5$  ms cadence.

Finally, to our knowledge, we have presented the highest time resolution search for intrinsic radio variability from a supermassive black hole to date. While intrinsic variability is not expected from 3C 84 due to its  $\sim 1$  hour light crossing timescale, we are unaware of any existing data that could rule out such behavior. Historically, astronomers didn’t expect interstellar scintillation, pulsars, or gamma-ray bursts, either.

The National Radio Astronomy Observatory is a facility of the National Science Foundation operated under cooperative agreement by Associated Universities, Inc. CAH acknowledges support from a Jansky Postdoctoral Fellowship from NRAO. We thank the following for support and helpful feedback: Tim Bastian, Walter Bricken, Paul Demorest, Vivek Dhawan, Chris Hirata, Amanda Kepley, Brian Mason, Toney Minter, Rick Perley, Richard Prestage, Alan Roy, and Craig Walker. We thank the anonymous referee for comments that led to the improvement of this work.

*Facilities:* VLA, GBT, SOHO, GOES.

## REFERENCES

- Abdo, A. A., Ackermann, M., Ajello, M., et al. 2009, ApJ, 699, 31
- Akahori, T., Ryu, D., & Gaensler, B. M. 2016, arXiv:1602.03235

- Akiyama, K., & Johnson, M. D. 2016, arXiv:1603.04880
- Armstrong, J. W., & Coles, W. A. 1978, *ApJ*, 220, 346
- Aleksić, J., Ansoldi, S., Antonelli, L. A., et al. 2014, *Science*, 346, 1080
- Berlin, A. B., Golnev, V. Y., Korolkov, D. V., et al. 1980, *Soviet Astronomy Letters*, 6, 322
- Bregman, J. N. 2007, *ARA&A*, 45, 221
- Brown, S., Farnsworth, D., & Rudnick, L. 2010, *MNRAS*, 402, 2
- Buote, D. A., Zappacosta, L., Fang, T., et al. 2009, *ApJ*, 695, 1351
- Braatz, J. 2009, Calibration of GBT Spectral Line Data in GBTIDL v2, [http://www.gb.nrao.edu/GBT/DA/gbtidl/gbtidl\\_calibration.pdf](http://www.gb.nrao.edu/GBT/DA/gbtidl/gbtidl_calibration.pdf)
- Cen, R., & Ostriker, J. P. 1999, *ApJ*, 514, 1
- Chang, P., Broderick, A. E., & Pfrommer, C. 2012, *ApJ*, 752, 23
- Chang, P., Broderick, A. E., Pfrommer, C., et al. 2014, *ApJ*, 797, 110
- Clarke, M. 1964, PhD thesis, Cambridge University
- Condon, J. J., Cotton, W. D., Greisen, E. W., et al. 1998, *AJ*, 115, 1693
- Cordes, J. M., & Wasserman, I. 2016, *MNRAS*, 457, 232
- Cordes, J. M., & Lazio, T. J. W. 2002, arXiv:astro-ph/0207156
- Davé, R., Cen, R., Ostriker, J. P., et al. 2001, *ApJ*, 552, 473
- Deng, W., & Zhang, B. 2014, *ApJ*, 783, L35
- Dennett-Thorpe, J., & de Bruyn, A. G. 2002, *Nature*, 415, 57
- Dent, W. A. 1966, *ApJ*, 144, 843
- Dietrich, J. P., Werner, N., Clowe, D., et al. 2012, *Nature*, 487, 202
- Dolag, K., Gaensler, B. M., Beck, A. M., & Beck, M. C. 2015, *MNRAS*, 451, 4277
- Donnert, J., Dolag, K., Lesch, H., & Müller, E. 2009, *MNRAS*, 392, 1008
- Fabian, A. C., Hu, E. M., Cowie, L. L., & Grindlay, J. 1981, *ApJ*, 248, 47

- Fabian, A. C., Sanders, J. S., Taylor, G. B., et al. 2006, MNRAS, 366, 417
- Fang H. X., Yang S. G., Wang S. C., Chin. Sci. Bull., 2012, 57, 3375
- Feldman, U., Landi, E., & Schwadron, N. A. 2005, Journal of Geophysical Research (Space Physics), 110, A07109
- Fender, R., & Oosterloo, T. 2015, MNRAS, 451, L75
- Gao, H., Li, Z., & Zhang, B. 2014, ApJ, 788, 189
- Garcia, H. A. 1994, Sol. Phys., 154, 275
- Génova-Santos, R., Atrio-Barandela, F., Kitaura, F.-S., & Mückel, J. P. 2015, ApJ, 806, 113
- Gralla, M. B., Crichton, D., Marriage, T. A., et al. 2014, MNRAS, 445, 460
- Haddock, F. T., & Sciama, D. W. 1965, Physical Review Letters, 14, 1007
- Harp, G. R., Ackermann, R. F., Astorga, A., et al. 2015, arXiv:1506.00055
- Hewish, A., Scott, P. F., & Wills, D. 1964, Nature, 203, 1214
- Hirata, C. M., & McQuinn, M. 2014, MNRAS, 440, 3613
- Haslam, C. G. T., Salter, C. J., Stoffel, H., & Wilson, W. E. 1982, A&AS, 47, 1
- Ioka, K. 2003, ApJ, 598, L79
- Keane, E. F., Johnston, S., Bhandari, S., et al. 2016, Nature, 530, 453
- Keane, E. F., & Petroff, E. 2015, MNRAS, 447, 2852
- Law, C. J., Bower, G. C., Burke-Spolaor, S., et al. 2015, ApJ, 807, 16
- Lieu, R., & Duan, L. 2013, ApJ, 763, L44
- Lieu, R., Duan, L., & Kibble, T. W. B. 2013, ApJ, 778, 73
- Lorimer, D. R., Bailes, M., McLaughlin, M. A., Narkevic, D. J., & Crawford, F. 2007, Science, 318, 777
- Lovelace, R. V. E., & Richards, D. W. 2013, MNRAS, 433, 2275
- Luan, J., & Goldreich, P. 2014, ApJ, 785, L26
- Maltby, P., & Moffet, A. T. 1962, ApJS, 7, 141



- Manoharan, P. K., & Ananthakrishnan, S. 1990, MNRAS, 244, 691
- Maoz, D., Loeb, A., Shvartzvald, Y., et al. 2015, MNRAS, 454, 2183
- Margalit, B., & Loeb, A. 2015, arXiv:1511.03615
- Marscher, A. P. 1979, ApJ, 228, 27
- Mason, B. S. 2013, Green Bank Telescope Memo #282
- Masui, K. W., & Sigurdson, K. 2015, Physical Review Letters, 115, 121301
- McMullin, J. P., Waters, B., Schiebel, D., Young, W., & Golap, K. 2007, Astronomical Data Analysis Software and Systems XVI, 376, 127
- McQuinn, M. 2014, ApJ, 780, L33
- McQuinn, M., Lidz, A., Zaldarriaga, M., et al. 2009, ApJ, 694, 842
- Mejia-Ambriz, J. C., Jackson, B. V., Gonzalez-Esparza, J. A., et al. 2015, Sol. Phys., 290, 2539
- Menzler, U., & Schlickeiser, R. 2015, MNRAS, 448, 3405
- Nagai, H., Asada, K., Doi, A., Kamenno, S., & Inoue, M. 2009, in ASP Conf. Ser. 402, Approaching Micro-Arcsecond Resolution with VSOP-2, ed. Y. Hagiwara, E. Fomalont, M. Tsuboi, & Y. Murata (San Francisco, CA: ASP), 106
- Pallottini, A., Ferrara, A., & Evoli, C. 2013, MNRAS, 434, 3293
- Palmer, D. M. 1993, ApJ, 417, L25
- Pauliny-Toth, I. I. K., Preuss, E., Witzel, A., et al. 1976, Nature, 259, 17
- Pedlar, A., Ghataure, H. S., Davies, R. D., et al. 1990, MNRAS, 246, 477
- Pen, U.-L., & Connor, L. 2015, ApJ, 807, 179
- Perley, R. A., & Butler, B. J. 2013, ApJS, 204, 19
- Robbrecht, E., & Berghmans, D. 2004, A&A, 425, 1097
- Ryle, M., & Windram, M. D. 1968, MNRAS, 138, 1
- Ryu, D., Schleicher, D. R. G., Treumann, R. A., Tsagas, C. G., & Widrow, L. M. 2012, Space Sci. Rev., 166, 1

- Shull, J. M., Smith, B. D., & Danforth, C. W. 2012, *ApJ*, 759, 23
- Smith, F. G. 1950, *Nature*, 165, 422
- Spitler, L. G., Scholz, P., Hessels, J. W. T., et al. 2016, *Nature*, 531, 202
- Taylor, G. B., Gugliucci, N. E., Fabian, A. C., et al. 2006, *MNRAS*, 368, 1500
- Tejos, N., Prochaska, J. X., Crighton, N. H. M., et al. 2016, *MNRAS*, 455, 2662
- Thornton, D., Stappers, B., Bailes, M., et al. 2013, *Science*, 341, 53
- Williams, P. K. G., & Berger, E. 2016, *arXiv:1602.08434*
- Wilman, R. J., Edge, A. C., & Johnstone, R. M. 2005, *MNRAS*, 359, 755
- Zheng, Z., Ofek, E. O., Kulkarni, S. R., Neill, J. D., & Juric, M. 2014, *ApJ*, 797, 71
- Zhou, B., Li, X., Wang, T., Fan, Y.-Z., & Wei, D.-M. 2014, *Phys. Rev. D*, 89, 107303

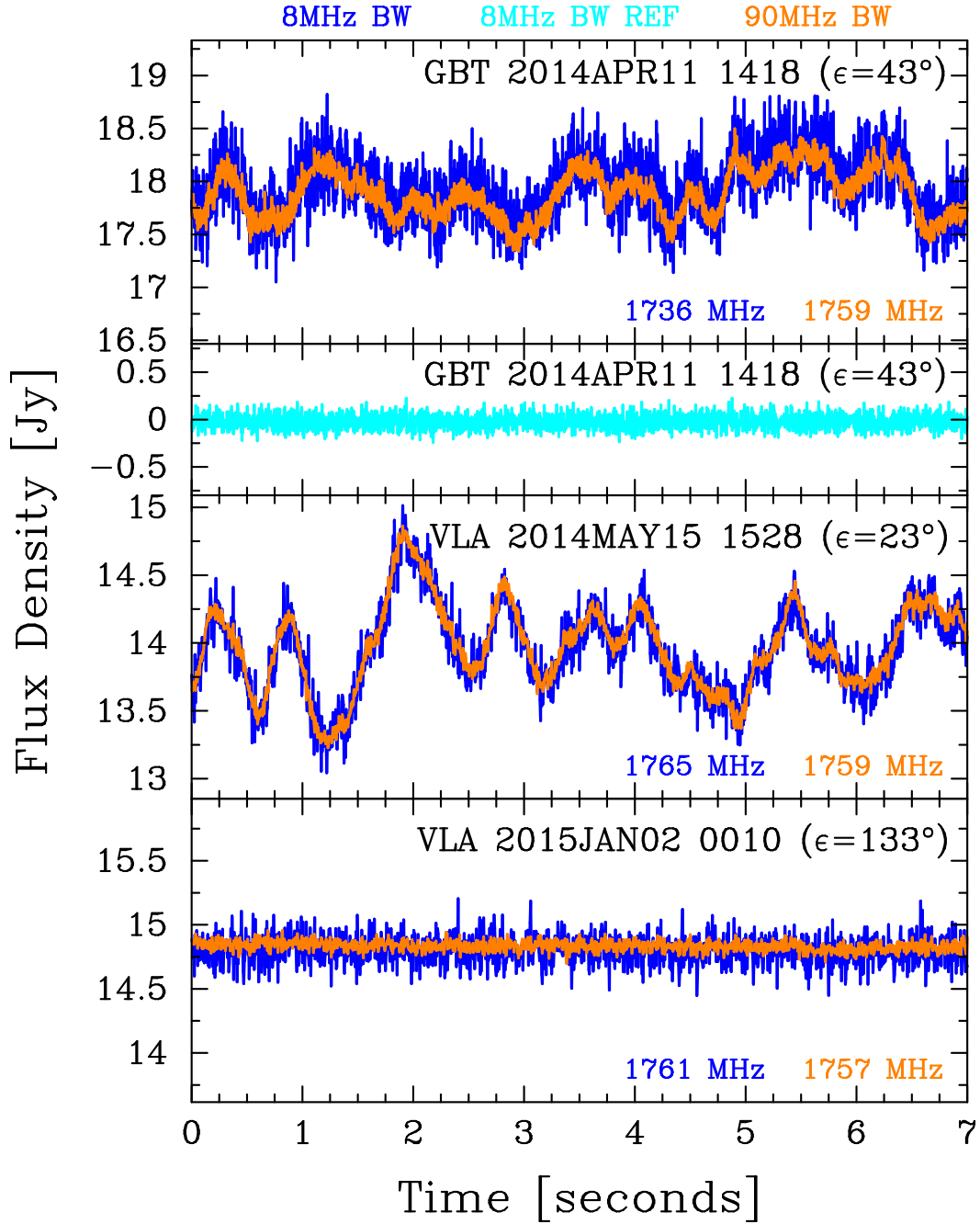


Fig. 1.— VLA and GBT light curves of 3C 84, spanning representative 7 s portions from observations at 3 epochs. The central frequencies of the 8 MHz (dark blue) and 90 MHz (orange) bandwidth data are indicated in each panel. The 8 MHz data for the GBT 3C 84 reference position is shown in the second panel (cyan). The range in each panel, except the second, spans  $\pm 8\%$  about the mean flux density of the 8 MHz data.

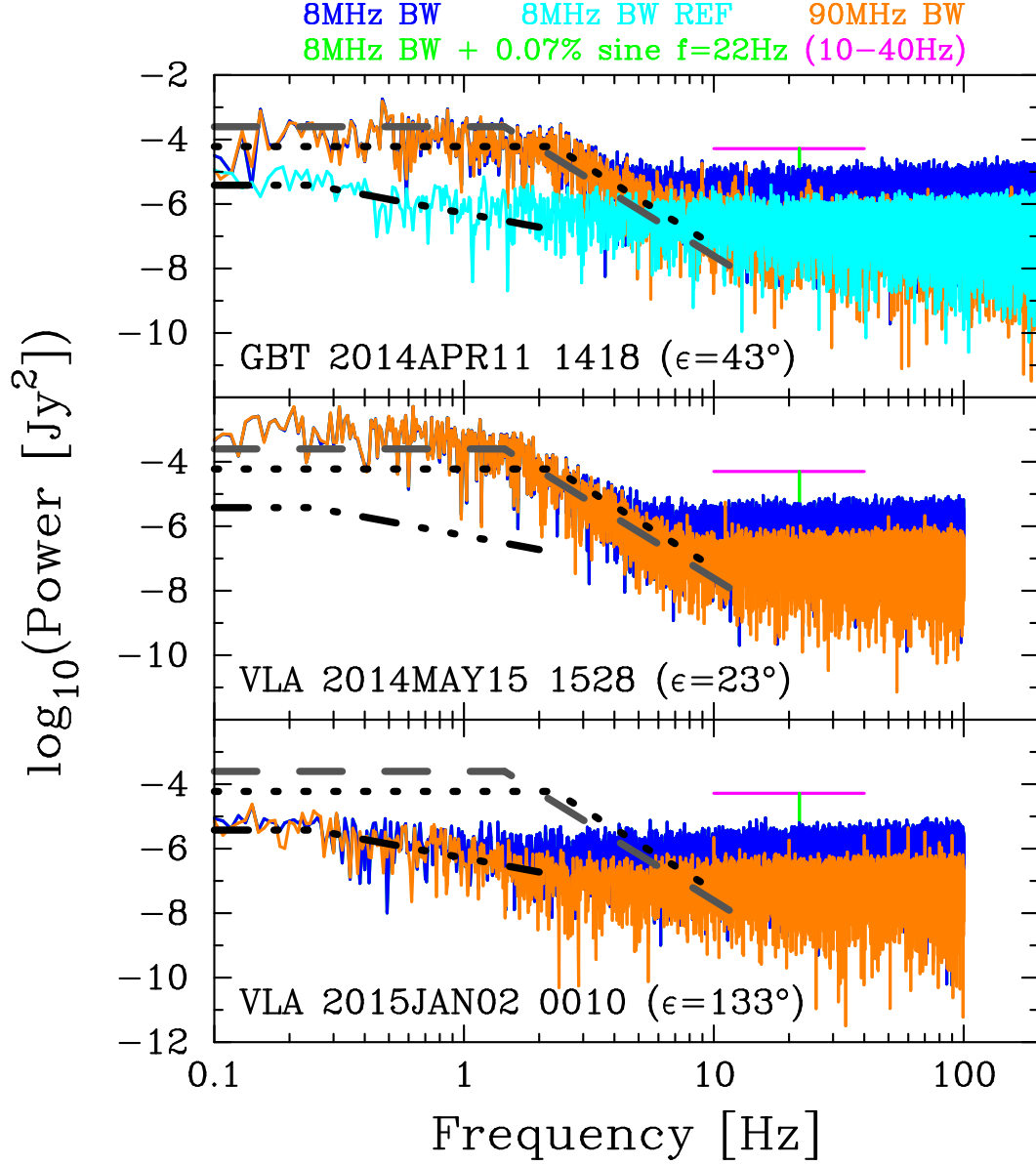


Fig. 2.— Temporal power spectra of light curves for 3C 84 at 3 epochs. The layout and color scheme matches Fig. 1. The 5 ms and 2.5 ms sampling of the VLA and GBT data permit examination to 100 Hz and 200 Hz, respectively. The dotted, dashed, and dot-dashed curves are informal fits characterizing the rise and plateau of spectra with decreasing frequency and are identical in each panel. See § 4 and § 5.2 for details. The green curve is calculated from the 8 MHz light curve at each epoch, but with a sinusoid added with period 22 Hz, mean intensity given by the mean of the original 8 MHz data, and standard deviation of fluctuations 0.05% (or wave amplitude 0.07%) of the mean intensity. The purple line indicates the power that would result for a similarly injected sinusoid with period between 10–40 Hz.